Available online at www.sciencedirect.com
ScienceDirect
Journal of Power Sources 180 (2008) 568–575
JOURNAL OF POWER SOURCES
www.elsevier.com/locate/jpowsour

The effect of $CoSn/CoSn_2$ phase ratio on the electrochemical behaviour of $Sn_{40}Co_{40}C_{20}$ ternary alloy electrodes in lithium cells

J. Hassoun [a,*], P. Ochal [a], S. Panero [a], G. Mulas [b], C. Bonatto Minella [b], B. Scrosati [a]

[a] *Department of Chemistry, University of Rome "La Sapienza", 00185 Rome, Italy*
[b] *Department of Chemistry, University of Sassari, I-07100 Sassari, Italy*

Received 17 December 2007; received in revised form 11 January 2008; accepted 22 January 2008
Available online 7 February 2008

Abstract

Samples of a SnCoC-based electrodes, all having the molar composition $Sn_{40}Co_{40}C_{20}$, but differing by the high energy ball milling synthesis conditions, have been tested in lithium cells. The investigation was carried out by using a series of complementary techniques, including potentiodynamic cycling with galvanostatic acceleration, galvanostatic charge–discharge cycling and impedance spectroscopy. The results confirmed the high capacity delivery of this type of ternary electrodes but also revealed that their electrochemical behaviour is influenced by the relative abundance of the nanosized domains of CoSn and $CoSn_2$ in their structure.

Keywords: Tin; Alloy; Ternary; Electrode; Lithium; Battery

1. Introduction

A Japanese manufacturer has recently announced the release on the market of a new Li-ion battery with the trade name of Nexelion [1,2]. Although the full composition has not yet been fully exposed, it has been reported that the battery employs non-conventional electrolyte and electrode materials, and in particular a novel tin amorphous ternary Sn–Co–C anode [3]. At a first sight, it is reasonable to suppose that this ternary electrode material operates on the basis of the "active/inactive medium" concept, namely that tin is the main electrochemical active component while the two other elements act principally as the supporting additives to buffer the volume expansion experienced by tin during the electrochemical process in a lithium cell. Indeed, it has been clearly reported that the volume variation, typically associated with the electrochemical Li-alloying process, can be effectively buffered by uniformly dispersing *in situ* or *ex situ* the electrochemically active element, *e.g.* Sn or Si, into a matrix of supporting components at nano-scale configuration [4–6].

However, in the case here under study it is expected that the role of cobalt and carbon may be more complex than that of solely providing a buffering action and, effectively, recent work of Dahn et al. [7] confirms this assumption. By a detailed structural and electrochemical investigation of a large number *of* ternary Sn–Co–C compositions, these authors have in fact evidenced a peculiar, multi-fold role of the carbon additive. Indeed, in addition to an improvement in conductivity, the carbon element also contributes to increase the specific capacity value, to stabilize the Li–Sn alloy at the atomic scale and to promote the nanostructure of the material during the synthesis. It has also been found that carbon incorporation during the synthesis of $Sn_{1-x}Co_x$ compounds is crucial for obtaining amorphous structures of the $[Sn_{0.55}Co_{0.45}]_{1-y}C_y$ type over the composition range of $0.28 < y < 0.43$ [8]. Also the third, Co component is expected to play an important role in these ternary compounds. In addition to buffer the principal volume expansion and thus, to prevent cracking of the electrode structure upon prolonged cycling, cobalt, being chemically inactive with carbon, also prevents the formation of intermetallic carbides over the entire useful composition range, thus avoiding the precipitation of tin out of the composite [7]. The same authors have shown that electrode based on a $Sn_{42}Co_{34}C_{24}$ composition can be cycled in lithium cells with a specific capacity value approaching 600 mA h g^{-1} [7] and that an increase of the carbon content

* Corresponding author.
E-mail address: jusef.hassoun@uniroma1.it (J. Hassoun).

0378-7753/$ – see front matter © 2008 Elsevier B.V. All rights reserved.
doi:10.1016/j.jpowsour.2008.01.059

up to 40% in the SnCoC composite further improved the capacity up to a value near 700 mA h g^{-1} [8].

Clearly, these results demonstrate that the Sn–Co–C-based materials are of practical interest in this paper and this accounts for their choice as innovative anodes in the Nexelion battery. However, these materials are also interesting in terms of fundamental properties since their electrochemical behaviour is not yet fully clear. This has encouraged us to carry out a detailed study of the Sn–Co–C ternary systems and, accordingly, in a previous work we have reported the results of an electrochemical investigation of electrodes having the $Sn_{31}Co_{28}C_{41}$ composition and prepared by low and high energy ball milling technique [9,10]. The results evidenced that the mechanical treatment conditions and the length of milling time employed for the synthesis played a key role for the achievement of the right phase composition with associated reflection on the electrochemical performance. Under the best conditions, the electrode provided a specific capacity of 500 mA h g^{-1} over 50 cycles.

In this paper we extend the investigation of the Sn–Co–C electrode system by examining the role of the reciprocal composition of the three components. In particular, we discuss the $Sn_{40}Co_{40}C_{20}$ case and report its electrochemical behaviour in function of the synthesis conditions.

2. Experimental

The Sn–Co–C samples were prepared by the ball milling technique. Commercial micrometric Sn (Johnson Mattey, 325 mesh, 99.8 purity), Co (GoodFellow 45 mesh e 99.8 purity) and C (Graphite, Aldrich) were used. For all samples, the formal Sn:Co:C molar ratio was 0.40:0.40:0.20, corresponding to a $Sn_{40}Co_{40}$ C_{20} stoichiometry.

Mechanical treatment was carried out employing a Spex Mixer-Mill mod. 8000, equipped with stainless steel vial and spheres. A powder charge of 8 g was treated with two 10 g balls. To prevent metal oxidation during milling, powder handling, as well as vial charging and sampling, were performed under a purified Ar atmosphere, in a MBraun glove box, with O_2 and H_2O content at ppm levels. Table 1 lists the samples prepared in this work and their different synthesis conditions.

The structure evolution of the samples was checked by XRD, using a Rigaku DMax diffractometer equipped with Cu Kα radiation and a graphite monochromator in the diffracted beam. The morphology was analysed by Scanning Electron Microscopy, SEM, using a SEM-EDS Leo 1450 VP.

The electrochemical response of the various $Sn_{40}Co_{40}C_{20}$ samples was tested in laboratory-type, lithium cells. The $Sn_{40}Co_{40}C_{20}$ working electrode was prepared as a thin film by doctor-blade deposition on a copper substrate of a slurry composed of 80% active material ($Sn_{40}Co_{40}C_{20}$), 10% PVdF 6020, Solvay Solef (binder) and 10% SP carbon (electronic support). A 1 M $LiPF_6$ in ethylene carbonate–dimethyl carbonate, EC:DMC 1:1 (Merck Battery Grade) solution soaked on a Whatman™ separator was used as the electrolyte and a lithium metal foil as the counter electrode. The cells were charged and discharged at various C-rate regimes (1 C corresponding to a current density value of 1.2 A cm^{-2} g^{-1}) and within a 0.01–1.5 V voltage limit. The electrochemical response of the cells was monitored by a Maccor Series 4000 Battery Test System.

The specific capacity of the $Sn_{40}Co_{40}C_{20}$ electrode was calculated considering both Sn and C as active elements, assuming the former as being involved in a lithium alloying–dealloying process:

$$4.4Li^+ + 4.4e^- + Sn = Li_{4.4}Sn, \quad (1)$$

and the latter in a lithium intercalation-deintercalation process:

$$Li^+ + e^- + 6C = LiC_6. \quad (2)$$

Under these conditions, the value of the theoretical specific capacity is given by $[(0.40 \times M_{Sn} \times 993 + 0.20 \times M_C \times 372)/0.679 \times M]$, where M_{Sn} = Sn molecular weight (118.7 g mol^{-1}), M_C = C molecular weight (12 g mol^{-1}) and $M = Sn_{0.40}Co_{0.40}C_{0.20}$ molecular weight (73.5 g mol^{-1}). Considering that there is 67.9 w:w.% of active elements (Sn, C) in 1 mol of $Sn_{0.40}Co_{0.40}C_{0.20}$, the resulting theoretical specific capacity is 963 mA h g^{-1} where the C contribution (related to the formation of LiC_6) is 18 mA h g^{-1}. The specific capacity of the material was calculated considering only the two active elements (Sn and C) excluding the electrochemically inactive Co to make a comparison compatible with that of compounds containing only electrochemically active elements such as SnC and Sn. This comparison allows to evaluate in our ternary compound the fraction of the active mass (especially Sn) participating in the reversible process.

The potentiodinamic cycling with galvanostatic acceleration (PCGA) was performed with a stepwise potential scans of 10 mV and a minimum current limits of 20 μA within a 0.01–1.5 V voltage limits using a VMP Biologic-Science Instruments in a three electrode cell where the $Sn_{0.40}Co_{0.40}C_{0.20}$ sample working film electrode was combined with a lithium counter electrode and lithium reference electrode. Also for this test the electrolyte was a 1 M $LiPF_6$ solution in an ethylene carbonate- dimethyl carbonate, EC:DMC 1:1 (Merck Battery Grade) electrolyte soaked on a Whatman™ separator.

Table 1
Milling time, phase and structural characteristics values of the samples examined in this work

Sample	Milling time (h)	CoSn/$CoSn_2$ weight (%)	CoSn domain size (nm)	$CoSn_2$ domain size (nm)
SnCoC I	38	42:58	13.6	14.8
SnCoC II	42	74:26	9.0	14.8
SnCoC III	54	91:9	11.0	13.0

All the samples have the same $Sn_{40}Co_{40}C_{20}$ formal composition and differ by the milling time. The CoSn/$CoSn_2$ weight % and the domain size values have been calculated by Maud software.

The impedance spectroscopy analysis was carried out by applying a 10 mV amplitude signal in the 50 kHz–0.005 Hz frequency range using a Frequency Response Analyzer (FRA) Schlumberger Solartron model 1260 coupled with EG&G Princeton Applied Research model 362 potentiostat. For this test we used a T-cell containing $Sn_{40}Co_{40}C_{20}$ as the working electrode and a lithium foil as the counter and the reference electrode. The impedance response was measured at different cycling stages, i.e., before cycling (in the OCV state, $V = 2.8$ V vs. Li^+/Li), after 5 cycles and after 100 cycles (in both cases at 1 C rate), see Fig. 6A–C.

3. Result and discussion

The electrochemical properties of the ternary Sn–Co–C electrode materials has been extensively studied by Dahn et al. [7]. These authors have clearly shown that the electrochemical activity in lithium cells is limited to some selected reciprocal compositions where the Sn–Co–C materials assume an amorphous, nano structure. In a previous work we have shown that nanostructured materials may be obtained within the same compositional ranges using a convenient, easy-to-perform ball milling technique [9,10]. Results obtained by ternary electrodes of the $Sn_{31}Co_{28}C_{41}$ stoichiometry demonstrated that the electrochemical response depended on the synthesis conditions and that under optimized preparation the electrodes could deliver a specific capacity of 500 mA h g^{-1}.

In the attempt to further enhance the capacity delivery, we have considered to increase the amount of the main electroactive element, namely the tin component, by synthesizing a new composition of formal $Sn_{40}Co_{40}C_{20}$ stoichiometry, i.e. a Sn-richer composition, however, still confined within the region where the Sn–Co–C system is expect to keep a nanostructured configuration [7].

In this investigation we have prepared three samples, all them having the $Sn_{40}Co_{40}C_{20}$ formal composition, but varying by the synthesis conditions in terms of milling time. Table 1 lists the samples examined in this work and their respective acronyms.

Fig. 1 reports the X-ray diffraction patterns of all three samples. The XRD pattern of the sample SnCoC I (see Table 1) reveals the signals which pertain to the CoSn and $CoSn_2$ phases. Both phases are characterized by few of easily distinguishable, separated marks (*e.g.* $2\theta = 28.5°$ for CoSn and $2\theta = 35.5°$ for $CoSn_2$), as well as by the section with merged peaks (2θ between 37° and 46°). The phases related to CoSn (JCPDS Library 02-0559) and $CoSn_2$ (JCPDS Library 25-0256) are hexagonal and tetragonal, respectively.

Each peak reveals a relatively high broadness, which suggests that the desirable nano-scaled morphology has been obtained. This was definitely confirmed by the Retvield analysis of the XRD patterns which demonstrated the nanocrystalline nature of the coherent diffraction domains for both phases and the corresponding relative amount. The results of the Retvield analysis with the determined average crystallite size, are summarized in Table 1.

Increasing the milling time under the same high energy conditions led to SnCoC II and SnCoC III, respectively, samples (see Table 1). Fig. 1 shows the corresponding evolution of the XRD pattern. Initially (sample SnCoC II), the peaks related to $CoSn_2$ decrease and the interval with merged peaks becomes more distinct, revealing that the CoSn phase content increases. The broadness of the peaks remains almost unchanged. The $CoSn_2$ peaks still decrease for sample SnCoC III. The CoSn/$CoSn_2$ phase ratio for the three samples is summarized in Table 1.

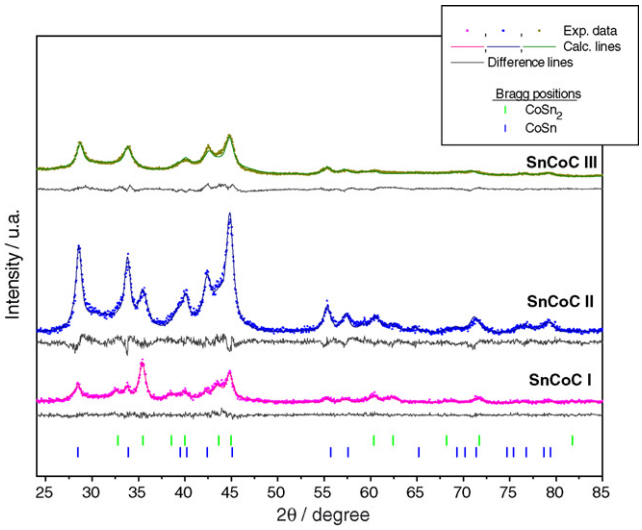

Fig. 1. XRD patterns of the three $Sn_{40}Co_{40}C_{20}$ samples prepared in this work. For sample identification see Table 1.

As it will be shown further on, these phase ratio and the nanosized features considerably influence the electrochemical behaviour of the SnCoC-based electrodes.

Fig. 2 shows the morphology of the three samples as revealed by SEM analysis. All samples show aggregated nanostructures with evident particle agglomeration. The grain size of the aggregates was estimated to range between hundred nanometers and few micrometers. To be noticed, however, that although agglomeration does occur, the nanodimension of the single particles is maintained in all the three cases.

The three samples were assembled in form of film electrodes and tested in a lithium cell to determine their electrochemical behaviour. Fig. 3 shows the evolution of a potentiodinamic cycling with galvanostatic acceleration (PCGA) tests carried out on the three samples prepared in this work. The peak evolution is similar for all the three cases, generally showing an initial activation cycle revealing a series of peaks in the cathodic scan which are not all reproduced in the following anodic scan. The first irreversible peak around 1.4 V vs. Li^+/Li is quite likely related to the formation of a passivating film (Solid Electrolyte Interface, SEI film) on the Sn surface, an extensive phenomenon usually observed for pure Sn electrodes [11]. However, in the case here under study, the peak has a low extension and this mild character suggests that the effect related to the surface film creation consistently decreased when passing from pure Sn to the ternary Sn–Co–C electrode. This confirms the importance of placing tin metal in a ternary matrix and of switching to the nano dimension for controlling the irreversible surface processes of tin-based lithium metal alloy electrodes. [11].

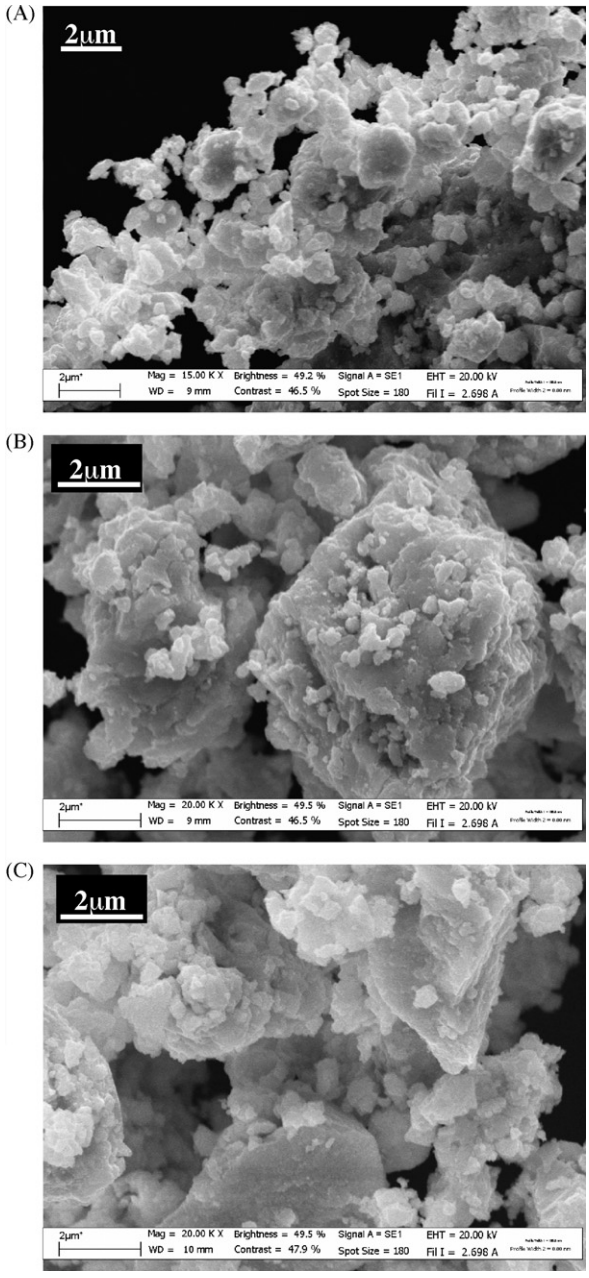

Fig. 2. SEM images of the three $Sn_{40}Co_{40}C_{20}$ samples prepared in this work. For sample identification see Table 1.

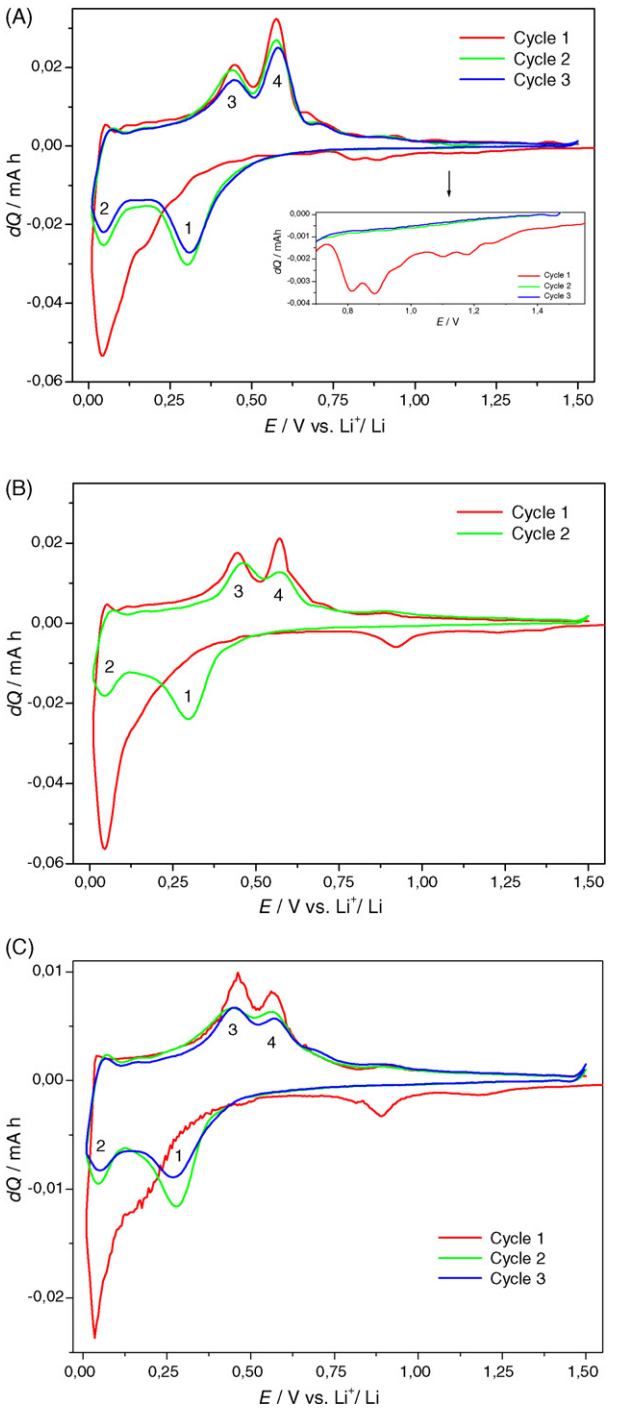

Fig. 3. PCGA test of the three $Sn_{40}Co_{40}C_{20}$ samples cycled in lithium cells. The results refer to: SnCoCI (A); SnCoCII (B) and SnCoc III (C). Electrolyte: EC:DMC 1:1 $LiPF_6$. Cyclic voltage limits: 0.01–1.5 V. Room temperature. For sample identification see Table 1.

The following peak in the first cathodic scan is observed at about 0.8 V vs. Li^+/Li, see Fig. 3. The voltage value and the related shape make this peak associable to additional electrolyte decomposition with a SEI film formation on the surface of the graphite component [12,13]. Further broad peaks appeared at low potentials, i.e., in the range of 0.4–0.01 V vs. Li^+/Li. They are likely due to the main electrochemical process which is the lithium alloying into the nanostructured phases. The profile and position of these peaks differ from those shown pure tin electrodes [14], this again being due to the complex matrix structure of the ternary Sn–Co–C electrodes here under consideration. In addition, the several steps which in the lithium alloying process of pure tin electrodes evolve over several steps, here overlap in two, large peaks occurring at about 0.3 V vs. Li^+/Li and 0.05 V vs. Li^+/Li, respectively.

In the anode scan of the first cycle only two distinguished peaks are observed and these peaks are consistently reproduced in the following cycles. The cycling regime becomes then repetitive with two peaks in the cathodic scan, marked as 1 and 2, reproduced in the anodic scan, marked as 3 and 4, see

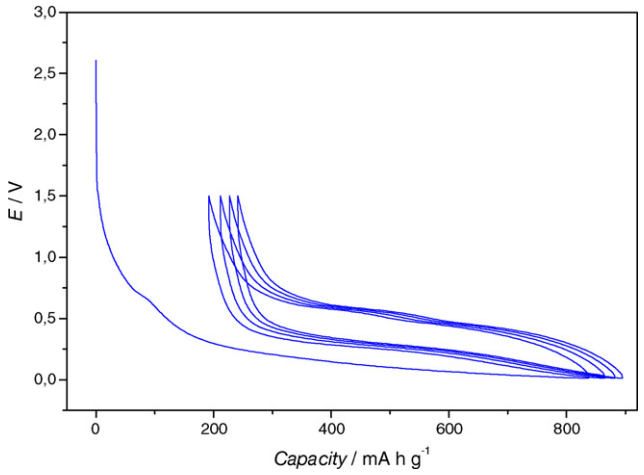

Fig. 4. Voltage vs. specific capacity profile of a Li/EC:DMC 1:1 $LiPF_6$/SnCoC I cell. Rate: C/4. Room temperature. For sample identification see Table 1.

Fig. 3. Obviously these reproducible behaviour represents the reversible process of the $Sn_{40}Co_{40}C_{20}$ electrode, where peaks 1 and 2 reflect the lithium alloying in tin and peaks 3 and 4 the opposite lithium de-alloying process, see processes (1). It cannot be excluded that these peaks also include the reversible partial lithium intercalation in the carbon matrix, see process (2).

This reversible process is typically reproduced in the charge–discharge voltage profile of a $Sn_{40}Co_{40}C_{20}$ electrode cycled in a lithium cell. Fig. 4 shows the case of the SnCoC I sample. A net capacity decay is observed passing from the first to the following cycles, this clearly being associated to the initial irreversible processes outlined by the PCGA results. However, the electrode quickly reaches a reproducible response with a reversible capacity approaching 600 mA h g^{-1}, i.e about 62% of the theoretical value assumed as 963 mA h g^{-1}, see experimental part. In the reversible charge–discharge behaviour, the voltage profile evolves with two distinguishable plateaus, which are associated to the reproducible peaks marked 1,2,3 and 4 in the PCGA curves. Very similar profiles were observed for cells using the SnCoC II and the SnCoC III sample electrodes.

Fig. 5 shows the response of the three sample electrodes upon prolonged cycling in lithium cells. Fig. 5A shows that the SnCoC I electrode delivers a specific capacity of the order of 600 mA h g^{-1}, a good fraction of which remains stable for many cycles. A continuous capacity decay and loss of efficiency, however, can be observed after the 30th cycle. This decay is quite likely associated with a progressive change upon cycling in the $CoSn_2$/CoSn phase ratio, as confirmed by *ex situ* XRD investigation of the cycled electrode (data not reported). Indeed, the $CoSn_2$ phase, theoretically richer in tin, is less stable than the CoSn phase. Moreover, we can assume that the capacity decay may also be due to a progressive loss of the electrical contact between the active Sn particles upon cycling, with consequent loss of electronic conduction paths with a resulting growth of the insulating parts in the matrix.

The cycling response of the sample SnCoC II electrode is shown in Fig. 5B. In this case the capacity continuously decay from an initial 650 mA h g^{-1} to a 400 mA h g^{-1} value in the course of 50 cycles. It is reasonable to suppose that the electrode undergoes a continuous phase transformation with associated decay in performance. This is confirmed by *ex situ* X-ray analysis which demonstrated that the $CoSn_2$ phase is indeed transformed during cycling into an amorphous structure, to which is associated a loss of electronic contact between the active particles (data not reported).

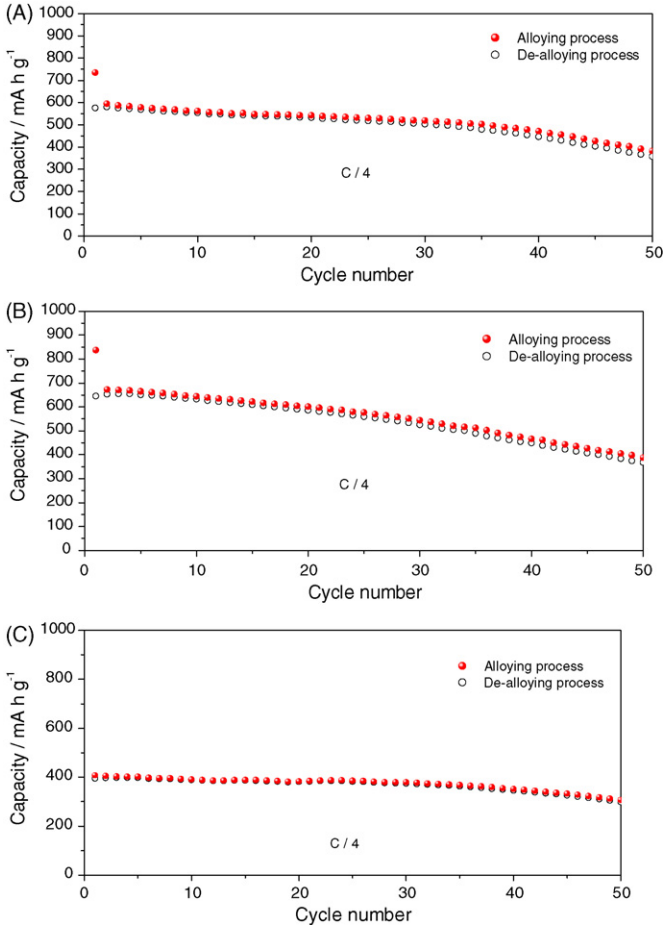

Fig. 5. Specific capacity vs. cycle number of lithium cells using SnCoC I (A); SnCoCII(B) and SnCoC III (C), respectively, samples as working electrodes. Electrolyte: EC:DMC 1:1 $LiPF_6$. Room temperature. For sample identification see Table 1.

The cycling response of the SnCoC III sample electrode, reported in Fig. 5C, differs from those observed for the other two electrode samples. The initial capacity of the SnCoC III electrode is lower, i.e. of the order of 400 mA h g^{-1}, in comparison with that of the samples SnCoC I and SnCoC II. This

Table 2
Significant impedance parameters associated to SnCoC II material cycle at 1 C rate in a lithium cell

State of the electrode	R_e (Ω)	R_{f1} (Ω)	R_{f2} (Ω)	R_{CT} (Ω)
OCV	1.7	3	22.3	–
After 5 cycles	4	1.8	2.5	16
After 100 cycles	3.8	2.8	12.3	16

Electrolyte: EC:DMC 1:1 $LiPF_6$. Re: electrolyte resistance, R_{f1}: first film resistance, R_{f2}: second film resistance, R_{CT}: charge transfer resistance.

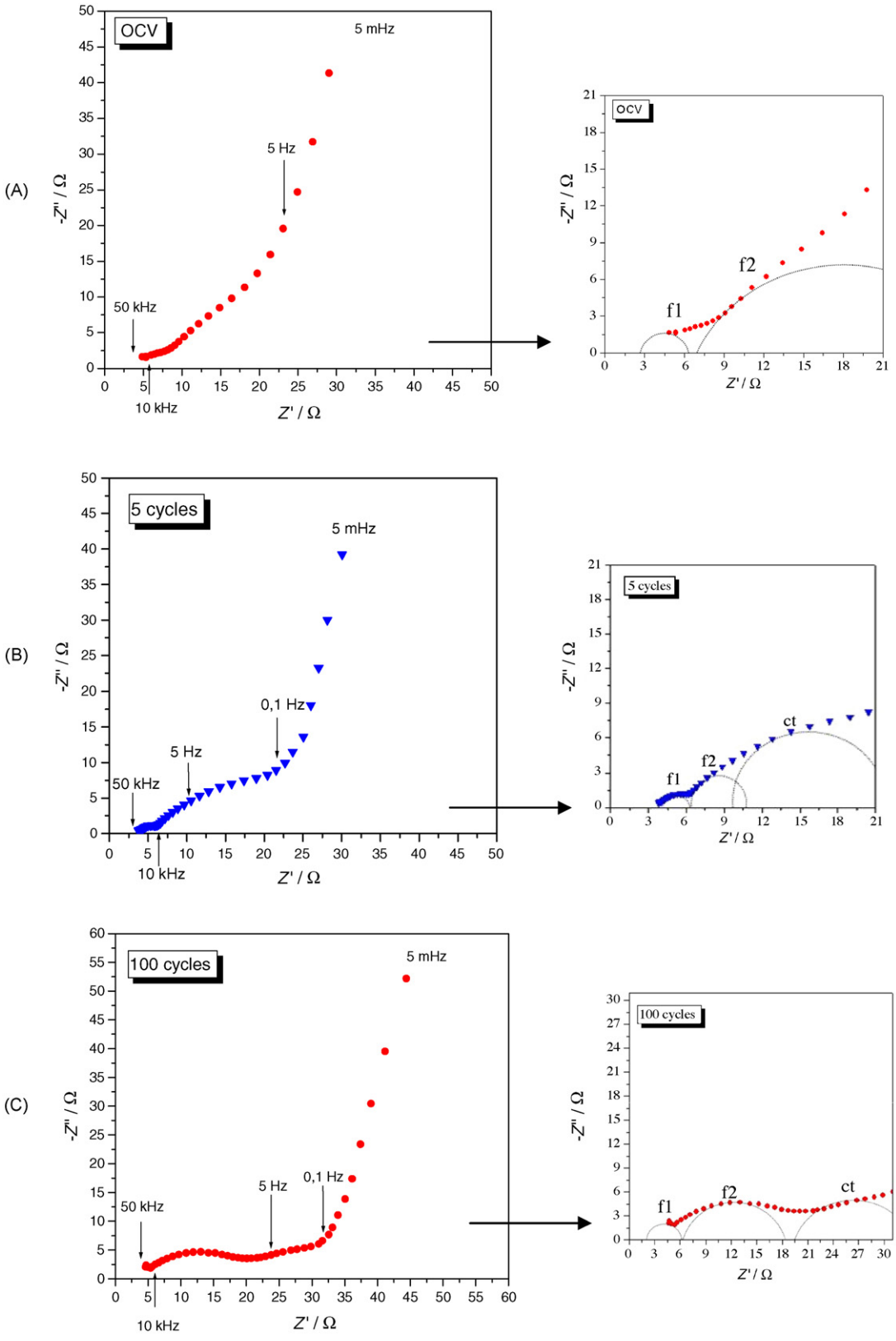

Fig. 6. Impedance response of a SnCoC/EC:DMC 1:1 $LiPF_6$/Li cell detected at different cycling stages, namely at OCV state, $V = 2.8$ V vs. Li^+/Li (A); after 5 cycles, $V = 1.4$ V vs. Li^+/Li (B) and, after 100 cycles, $V = 1.3$ V vs. Li^+/Li (C). Rate: 1 C. Room temperature. The right side of the figure shows an approximate overlapping of the experimental data and the circuital elements as determined by the fitting analysis in the high (10 kHz–50 kHz) and medium–high (0.1 Hz–10 kHz) frequency ranges.

difference can be attributed to the large predominance in the sample SnCoC III of the CoSn phase, i.e. richer in the electrochemically inactive Co, a fact which may induce a decrease of the Sn active fraction due to the creation of Sn grains hidden to lithium ions. However, considering the higher electrochemical stability of the CoSn phase, the capacity retention upon cycling of the samples SnCoC III is much higher than that observed for SnCoC I and SnCoC II, compare Fig. 5C with Fig. 5A and B.

To shed more light on the electrochemical behaviour of the Sn–Co–C electrodes we have performed an impedance spectroscopy analysis run at different cycles, i.e, at cycle 0 (under open circuit, OCV, conditions), after 5 charge–discharge cycles and after 100 charge–discharge cycles. The voltage values were 2.8 V vs. Li^+/Li at the OCV state, 1.4 V vs. Li^+/Li after 5 cycles and 1.3 V vs. Li^+/Li after 100 cycles.

The general response may be qualitatively described in terms of two semicircles, followed by a low frequency tilted line. The low frequency region (5 mHz–0.1 Hz), likely corresponding to cell geometric capacitance [11,15], remains almost unchanged for all the three cycling stages. A meaningful difference, however, is observed in the medium–high frequency region. To properly interpret the responses in this region, the data sets were analysed by a non-linear least-square (NLLSQ) fit software developed by Boukamp [16,17] based on the equivalent circuit $R_e(R_{f1}Q_{f1})(R_{f2}Q_{f2})Q_g$ at 0 cycle and on the equivalent circuit $R_e(R_{f1}Q_{f1})(R_{f2}Q_{f2})(R_{CT}Q_{CT})Q_g$ after 5 and 100 charge–discharge cycles. The matching with the experimental data were quite good as confirmed by a chi-square factor of the order of 10^{-4}, which is considered as an acceptable prerequisite to the validity of the proposed circuitry model. Table 2 shows the impedance value determined at the three examined cycling stages.

In the plot recorded before the cycling test, i.e. at the OCV state (see Fig. 6A), the impedance response can be easily fitted by two semicircles, marked as f1 and f2, which seem to be related to the formation of complex native films on the electrode surface. The occurrence of passivation film on the Sn surface was indeed demonstrated by Dahn and co-workers [18,19]. It is reasonable to assume that this film is formed on the surface of tin, as well as on that of graphite, just after the cell assembling. More complicated is the interpretation of the spectra recorded after cycling. The spectrum at 5 cycles (see Fig. 6B) exhibits three semicircles, i.e., a single one distinguishable at high frequency (10 kHz–50 kHz) and two convoluted ones in the medium–high frequency region (0.1 Hz–10 kHz). The fitting analysis suggests that the high frequency semicircle, marked as f1, is probably due to the above discussed native film resistance. The amplitude of this semicircle does not change significantly after 5 cycles. The other two medium–higher frequency semicircles are related to a combination of film resistance, R_{f2}, and charge transfer R_{CT}. This interpretation is supported by the associated capacitance values, which are of the order of 10^{-5} F, i.e. a value typically associated to surface films, and of 10^{-3} F, i.e a value typically associated to charge transfer phenomena. The amplitude the second semicircle related to the electrode film, f2, decreases after 5 cycles, probably because of a partial interface cracking due to the volume stress associated to the lithium insertion–deinsertion processes.

Apparently similar is the impedance response recorded after 100 cycles, see Fig. 6C. However, the detailed analysis reveals a significant increase of the medium high frequency semicircle f2, related to the electrode film, this suggesting a series of complex phenomena at the electrode surface, involving multiple cracking and rebuilding of the film, this resulting in a continuous evolution of the whole interface region. These impedance results account for the progressive loss of capacity experience by the SnCoC II sample upon cycling in a lithium cell, see Fig. 5B. However, the impedance test also reveals that even for this electrode, the charge transfer resistance does not change upon cycling (see Table 2), this further confirming the role of the two additional Co and C components in stabilizing the electrochemical process of Sn-based electrodes.

4. Conclusions

The main goal of this work was the investigation of the electrochemical behaviour of Sn–Co–C ternary electrodes supposedly similar to those used in a battery recently marketed by a Japanese company. The results obtained on a material having the $Sn_{40}Co_{40}C_{20}$ composition and prepared by high-energy ball milling, show that this type of electrodes have a high specific capacity and a good electrolyte/electrode interface stability. We also show that the delivered specific capacity and the cycle life are strongly related to the value of the $CoSn/CoSn_2$ phase ratio, as well as on the nanocrystalline nature of the electrode material. Future work will be addressed to systems with different compositions to complete the investigation of the role of the various phases in influencing the electrochemical performance of this interesting class of materials so as to finally establish the effective practical relevance of these ternary compounds.

Acknowledgments

This work has been carried out with the financial support of the Italian Ministry of University and Research under a PRIN 2005 project. One of the authors, P. Ochal, thanks the European Network of Excellence (ALISTORE) for a thesis grant.

References

[1] S. Kawakami, M. Asao, US Patent No. 6,949,312 (2005).
[2] S. Mizutani, H. Inoue, US Patent Application, Publication No.0208378 (2005).
[3] H. Inoue, International Meeting on Lithium Batteries, IMLB 2006, June 18–23, 2006, Biarritz, France (abstr.# 228).
[4] O. Mao, R.A. Dunlap, J.R. Dahn, J. Electrochem. Soc. 146 (1999) 405.
[5] O. Mao, R.A. Dunlap, J.R. Dahn, J. Electrochem. Soc. 146 (1999) 414.
[6] O. Mao, R.A. Dunlap, J.R. Dahn, J. Electrochem. Soc. 146 (1999) 423.
[7] J.R. Dahn, R.E. Mar, A. Abouzeid, J. Electrochem. Soc. 154 (2007) A597.
[8] J.R. Dahn, R.E. Mar, A. Abouzeid, J. Electrochem. Soc. 153 (2006) A361.
[9] J. Hassoun, G. Mulas, S. Panero, B. Scrosati, Electrochem. Comm. 9 (2007) 2075.
[10] J. Hassoun, S. Panero, G. Mulas, B. Scrosati, J. Power Sources 171 (2007) 928.

[11] J. Hassoun, P. Reale, S. Panero, J. Power sources 174 (2007) 321.
[12] D. Aurbach, B. Markovsky, M.D. Levi, E. Levi, A. Schechter, M. Moshkovich, Y. Cohen, J. Power Sources 81/82 (1999) 95.
[13] J.O. Besenhard, M. Winter, J. Yang, W. Biberacher, J. Power Sources 54 (1995) 228.
[14] J. Hassoun, S. Panero, P. Reale, B. Scrosati, Int. J. Electrochem. Sci. 1 (2006) 110.
[15] J.R. McDonald, Impedance Spectroscopy, Wiley, New York, 1987.
[16] B.A. Boukamp, Solid State Ionics 18 (1986) 136.
[17] B.A. Boukamp, Solid State Ionics 20 (1986) 31.
[18] S.D. Bettie, T. Hatchard, A. Bonakdarpour, K.C. Hewitt, J.R. Dahn, J.Electrochem. Soc. 150 (2003) A701.
[19] L.Y. Beaulieu, S.D. Bettie, T. Hatchard, J.R. Dahn, J. Electrochem. Soc. 150 (2003) A419.